

OPEN ACCESS

Editors' Choice—Rapid Deactivation Convolutes Electrochemical CO₂ Reduction Selectivity Measurements on Gold Rotating Ring Disk Electrodes

To cite this article: Maria Kelly *et al* 2025 *J. Electrochem. Soc.* **172** 046503

View the [article online](#) for updates and enhancements.

You may also like

- [A Novel One-Step Electrochemical Sensor Utilizing Au–Ni Nanoparticles Supported on Etched MOF Nanocomposite for Rapid and Highly Sensitive 3–Nitrophenol Detection](#)

Lanyue Wang, Beibei Wang, Kai Kang et al.

- [Electrochemical Survey of Ln³⁺ \(Ln = Dy, Er, Gd, Ho, Tb, Tm\) in a Bis\(trifluoromethylsulfonyl\)imide-Based Room-Temperature Ionic Liquid with and without Added Chloride Ion](#)

Heather Hamilton and Charles L. Hussey

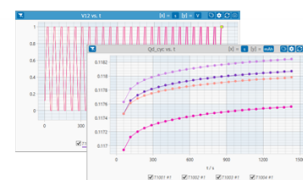
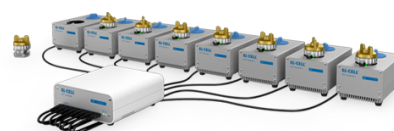
- [Advanced Multi-Cell Housing Designs to Prevent Thermal Runaway Propagation in Lithium-Ion Batteries](#)

Rengaswamy Srinivasan, Bliss G. Carkhuff, Hicham Alkandry et al.

PAT-Tester-x-8 Potentiostat: Modular Solution for Electrochemical Testing!

 electrochemical test equipment

- ✓ **Flexible Setup with up to 8 Independent Test Channels!**
Each with a fully equipped Potentiostat, Galvanostat and EIS!
- ✓ **Perfect Choice for Small-Scale and Special Purpose Testing!**
Suited for all 3-electrode, optical, dilatometry or force test cells from EL-CELL.
- ✓ **Complete Solution with Extensive Software!**
Plan, conduct and analyze experiments with EL-Software.
- ✓ **Small Footprint, Easy to Setup and Operate!**
Usable inside a glove box. Full multi-user, multi-device control via LAN.



Contact us:

☎ +49 40 79012-734

✉ sales@el-cell.com

🌐 www.el-cell.com



Editors' Choice—Rapid Deactivation Convolutes Electrochemical CO₂ Reduction Selectivity Measurements on Gold Rotating Ring Disk Electrodes

Maria Kelly,^{1,2,3,*} Rachel A. Wnuk,³ Recep Kas,³ Glenn Teeter,⁴ Melissa E. Kreider,^{3,**} and Wilson A. Smith^{1,2,3,z}

¹Department of Chemical and Biological Engineering, University of Colorado Boulder, Boulder, Colorado 80309, United States of America

²Renewable and Sustainable Energy Institute, University of Colorado Boulder, Boulder, Colorado 80309, United States of America

³Chemistry and Nanoscience Center, National Renewable Energy Laboratory, Golden, Colorado 80401, United States of America

⁴Materials Sciences Center, National Renewable Energy Laboratory, Golden, Colorado 80401, United States of America

Voltammetric measurements of electrochemical CO₂ reduction reaction (CO₂RR) selectivity on rotating ring disk electrodes (RRDE) are a rapid and sensitive method for quantifying an electrocatalyst's selectivity, i.e. faradaic efficiency (FE). This method has been applied to polycrystalline Au electrocatalysts where a Au disk electrode catalyzes both the CO₂RR and hydrogen evolution reaction while the concentric Au ring electrode selectively senses CO by oxidizing CO back to CO₂. Such measurements enabled fundamental mechanistic studies but suffer from poor inter-laboratory reproducibility. This work identifies causes of variability in RRDE selectivity measurements by comparing protocols with different electrochemical methods, reagent purities, and glassware cleaning procedures. We observed FE_{CO} decrease by 56% during 5 min chronoamperometry measurements, a phenomenon that is not readily apparent in voltammetric scans due to their dynamic nature. Electroplating of electrolyte impurities onto the disk and ring surfaces were identified as a major contributor to Au deactivation. Additionally, the oxygen reduction reaction may lead to higher disk currents in inadequately purged electrolytes, causing an apparent underestimation of FE_{CO} at low overpotentials. Lastly, we propose operational bounds for CO₂RR selectivity measurements on Au using the RRDE method and provide suggestions on steps for improving the accuracy of this technique.

© 2025 The Author(s). Published on behalf of The Electrochemical Society by IOP Publishing Limited. This is an open access article distributed under the terms of the Creative Commons Attribution 4.0 License (CC BY, <https://creativecommons.org/licenses/by/4.0/>), which permits unrestricted reuse of the work in any medium, provided the original work is properly cited. [DOI: 10.1149/1945-7111/adc553]



Manuscript submitted October 24, 2024; revised manuscript received March 3, 2025. Published April 9, 2025.

Supplementary material for this article is available [online](#)

Combining renewable electricity with chemical manufacturing via electrochemical processes provides a path for electrification of the chemical industry.^{1–3} One such process, the electrochemical CO₂ reduction reaction (CO₂RR), converts CO₂ to higher value products using an electrocatalyst.³ Typically, Ag or Au catalysts are used for carbon monoxide production, Sn for formate, and Cu for multi-carbon products such as ethylene and ethanol.^{3,4} Industry, governments, and academic institutions are currently researching CO₂RR as a pathway to carbon neutral chemicals and fuels.

A key performance metric for CO₂RR catalysts is selectivity for a single chemical product.⁵ Selectivity is often represented by a catalyst's faradaic efficiency (FE), that is, the number of electrons that go toward producing a specific product divided by the total number of electrons passed during electrolysis. Catalysts targeting CO, HCOOH, or C₂H₄ production will likely require >80% FE for industrial applications due to the high costs of separations.⁶ However, a major challenge for CO₂RR catalyst development is suppressing the competing hydrogen evolution reaction (HER) that is often favored under the same reaction conditions for CO₂RR in aqueous electrolytes. Thus, it is important to develop experimental techniques to measure the selectivity of a given catalyst for CO₂RR and HER under well-defined experimental conditions.

Gas and liquid chromatography are frequently used to quantify CO₂RR products.⁷ However, these chromatography techniques have long response times and require accumulation of sufficient sample volume, resulting in time resolutions of minutes to hours.^{8,9} The selectivity data is averaged over a long time period (e.g. minutes) compared to the sampling rate of electrochemical data, which is on the

order of μ s to ms for typical potentiostats.^{10,11} Rotating ring disk electrode (RRDE) experiments are an alternative method for real-time product detection and selectivity quantification with negligible time delays for CO₂RR.^{8,9,12–19} In addition, RRDE experiments are easy to set up, cost-effective, and provide exceptional mass transport control.

An RRDE consists of two concentric but electrically isolated electrodes: one central disk and an outer ring that are separated by an insulator such as poly(tetrafluoroethylene) (PTFE) or poly(ether-etherketone) (PEEK), as shown in Fig. 1. The RRDE is attached to a rotating shaft and immersed in the electrolyte of interest. The controlled rotation of the RRDE at a fixed rate, ω , produces a constant flux of fresh electrolyte to the electrode surface under well-defined mass transport conditions.²⁰ Two primary modes of RRDE operation have been presented in literature for product detection. The first is to operate the disk at a constant potential while cycling the ring potential (ring-scan mode).^{9,13,17,21} This allows for detection of the disk's reaction products by their electrochemical redox signatures in the ring's cyclic voltammogram. Ring-scan mode is particularly useful if the catalyst produces multiple products with unique electrochemical reactivity that can be identified separately; however, it is not possible to quantify FEs. The second mode of RRDE operation is to cycle the disk potential while holding the ring potential constant (disk-scan mode).^{8,12–15,18} The ring is set to a potential where the oxidation of a specific CO₂RR product is mass transport limited. In addition to product detection, the ring material can be selected to enable measurements of local pH (e.g. IrO_x or Au functionalized by a pH sensing molecule),^{16,21–23} however, such measurements are outside the scope of this article.

In the case of disk electrodes that produce only CO and H₂, the disk catalyzes CO₂RR and HER while the ring electrochemically senses the CO coming off the disk by oxidizing CO back to CO₂. The ring material must be carefully selected to provide the desired CO detection response. At the selected ring potential, E_{ring} , the material must:

*Electrochemical Society Student Member.

**Electrochemical Society Member.

^zE-mail: Wilson.Smith@nrel.gov

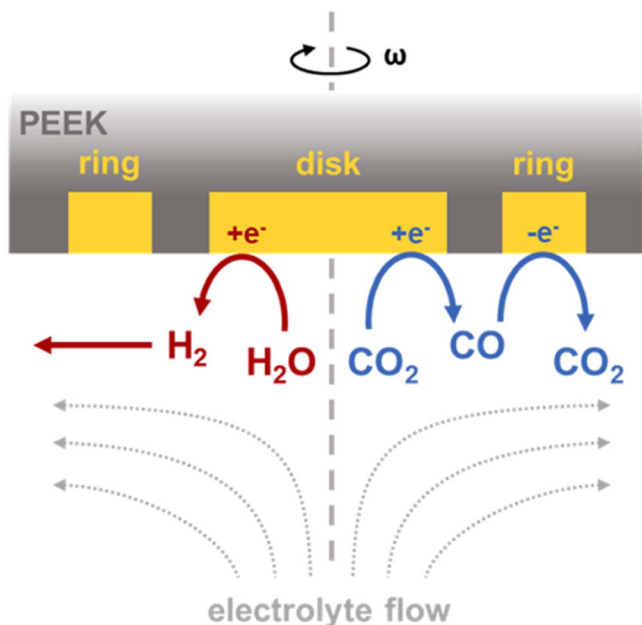


Figure 1. Schematic of a Au/Au RRDE cross-section. The Au disk catalyzes CO₂RR and HER. The Au ring catalyzes CO oxidation but not H₂ oxidation. The electrode rotates at rate ω , causing the electrolyte to flow in streamlines shown by the dotted gray lines.

1. Have a reproducible CO oxidation response without being poisoned
2. Be mass transport limited in the CO oxidation reaction (COOR) to prevent kinetic effects from influencing the ring's current response
3. Not react with H₂ or any other solution species

Polycrystalline Au (poly-Au) meets all these criteria, making it a common ring material for CO detection. Disk-scan mode measurements on poly-Au RRDEs can quantitatively determine CO₂RR FEs as first demonstrated by Goyal et al. in CO₂ saturated 0.1 M NaHCO₃.¹⁴ The authors used the subtraction method^{24,25} to quantify FE_{CO} and FE_{H₂} in the potential range -0.4 to -0.8 V vs RHE. In a subsequent work, the researchers used the same RRDE technique to deduce the dominant proton donor for HER in three different potential regimes.¹⁵

However, the reproducibility of quantitative disk-scan mode studies on poly-Au across different laboratories is quite poor. Literature reports under the same conditions (0.1 M NaHCO₃, poly-Au/Au RRDE, $E_{\text{disk}} = -0.6$ V vs RHE) found FE_{CO} can range from 66%–78% at 1600 rpm and 50%–83% at 2500 rpm as summarized in Table S1 of the Supplementary Information (SI).^{14–16,18,26} For comparison, seminal work by Hori et al. benchmarked the selectivity of poly-Au for CO at FE_{CO} = 87.1% (0.1 M KHCO₃, $E = -0.74$ V vs RHE) in an H-cell (no forced convection).⁴

Cui et al. attributed the variability of RRDE selectivity measurements to the presence of metal electrolyte impurities that, in their study, resulted in a 10.7% FE_{CO} decrease.²⁶ Deactivation of poly-Au during CO₂RR is frequently attributed to electroplating of Cu, Pb, Zn and/or Fe from bicarbonate electrolytes, even when using high purity ($\geq 99.9999\%$) reagents.^{26–28} Accumulation of these trace metals, which may only be present at ppb levels, on low surface area electrodes can significantly enhance their selectivity toward H₂ and other CO₂ reduction products at the expense of CO production.²⁹ However, Wuttig and Surendranath showed that pre-treatment of electrolytes with metal complexing agents (i.e. ethylenediaminetetraacetic acid or Chelex resin) effectively removes trace metal impurities and eliminates deactivation of poly-Au electrodes (2 h

of electrolysis at -0.7 V vs RHE in purified 0.1 M NaHCO₃).²⁷ Electrolytes can also be purified by pre-electrolysis wherein metal contaminants are plated onto a sacrificial electrode for several hours.³⁰ However, pre-electrolysis has been criticized for being less effective and time-consuming when compared to metal complexation pre-treatment methods.^{27,31}

Deactivation of CO₂RR catalysts is also observed even when trace metal impurities are not detected. Proposed mechanisms include adsorption of organic intermediates and impurities^{30,32,33} or further reduction of CO₂RR products to graphitic carbon layers.^{34,35} Since these “poisons” arise primarily from CO₂RR itself, electrolyte pre-purification is ineffective at addressing these deactivation routes. Instead, periodic anodic stripping procedures have been applied to re-activate the electrode surfaces.^{31,36}

Measurements of deactivation and its impact on RRDE selectivity measurements have not been extensively reported despite being a common and deleterious occurrence for CO₂RR on poly-Au. This article investigates the factors influencing deactivation rates on poly-Au/Au RRDEs for CO₂RR and their impact on quantitative selectivity measurements. We primarily employed chronoamperometry (CA) to deconvolute the effects of deactivation and changing electrode potential on FE_{CO}. We consistently observed rapid decrease in both CO selectivity at the disk electrode and CO detection at the ring electrode over just 5 min. Periodic anodic stripping treatments on both the ring and disk were necessary to recover the initial CO selectivity and detection sensitivity of the RRDE.

Despite implementing proven electrolyte and glassware cleaning protocols,^{27,37} the deactivation rate is only reduced by ca. 30%–40%, indicating that multiple deactivation mechanisms may be at play in addition to contamination by trace metals and organic compounds. We discuss the importance of measuring and correcting for Au deactivation during RRDE measurements to avoid erroneous mechanistic conclusions. To support the development of a robust, reproducible electroanalytical method, further study and, ideally, elimination of these deactivation routes on poly-Au/Au RRDEs are necessary.

Experimental

Materials and chemicals.—Electrocatalysts consisted of a poly-Au RDE (embedded in a PTFE shroud, E5 Series, Pine Research) or a poly-Au/Au RRDE (embedded in a PEEK shroud, PEEK spacer between ring and disk, E6R2 Series, Pine Research). Experiments requiring subsequent surface characterization used a poly-Au RDE with a removeable disk (PTFE shroud, ChangeDisk E5TQ Series, Pine Research). Deionized (DI) water (>18.2 M Ω -cm, TOC <5 ppb) from a Milli-Q system (Millipore) was used for electrochemical cell storage, electrode polishing, and electrolyte preparation. Unless otherwise noted, all glassware was cleaned by a laboratory dishwasher (PG 8535, Miele) using potassium hydroxide (pH = 12.3 to 12.8, Dr Weigert neodisher laboclean FLA) and citric acid (pH = 2.6 to 3.0, Dr Weigert neodisher Z) detergents following the INORGANICA wash protocol.³⁸ An alternative glassware cleaning procedure used an oxidizer salt (Alnochromix, Alconox Inc.) and sulfuric acid (98%, Veritas redistilled, GFS Chemicals) as described in section S2, SI.³⁷ Polycrystalline diamond suspensions (3 μm , 1 μm , and 0.25 μm , MetaDi, Buehler), acetone (99.5%, ACS grade, Fisher), and nitric acid (69.5%, Veritas Trace, GFS Chemicals) were used for electrode polishing. Electrolytes were prepared using sulfuric acid (98%, Veritas redistilled, GFS Chemicals), NaHCO₃ ($\geq 99.7\%$, ACS grade, Fisher), Na₂CO₃ ($\geq 99.999\%$, TraceSELECT, Honeywell), and Chelex 100 Resin (sodium form, 50–100 mesh, analytical grade, Bio-Rad). Poly-dopamine coating of electrodes used dopamine HCl (Sigma Aldrich), Na₂HPO₄ ($\geq 99.0\%$, ACS grade, Sigma Aldrich), and NaH₂PO₄·H₂O ($\geq 99.0\%$, ACS grade, Sigma Aldrich). RRDE collection efficiencies were determined using K₃Fe(CN)₆ ($\geq 99.0\%$, ACS grade, Sigma Aldrich). N₂ (99.9999%, research purity, Matheson), CO (99.999%, research

purity, Matheson), CO₂ (99.8%, bone dry), and H₂ (99.999%, ultra high purity, Matheson) were used to purge and blanket the electrolytes.

Instrumentation.—Electrochemical measurements were conducted with a CH Instruments 760E bipotentiostat and Electrochemical Workstation software. Solution pH was measured by an Oakton 700 pH meter calibrated daily by pH 4, 7, and 10 standard buffers (Hanna Instruments). X-ray photoelectron spectroscopy (XPS) measurements were collected by a Physical Electronics PHI Versa Probe III XPS with an Al K α X-ray source. The binding energy scale was calibrated using Cu 2p_{3/2} (932.62 eV) and Au 4f_{7/2} (83.96 eV) core levels measured on sputter-cleaned foils. Peaks were fitted using Gaussian-Lorentzian shapes with a Shirley background. Elemental compositions were calculated from XPS data by normalizing background-corrected peak areas by elemental sensitivity factors. Scanning electron microscopy (SEM) images and energy dispersive spectroscopy (EDS) maps were collected on a Hitachi 4800 SEM equipped with an EDS detector (Model No. 4473C-3UPS-SN, Thermo Fisher) or a Thermo Fisher Nova 360 SEM equipped with an EDS detector (Ultim Max 170, Oxford Instruments). SEM images and EDS maps were acquired with accelerating voltages of 7.0 kV and 15 kV. Inductively coupled plasma mass spectrometry (ICP-MS) measurements were conducted using a Thermo Scientific iCAP Q instrument in kinetic energy discrimination mode using He cell gas. Aliquot samples taken from the electrolyte were diluted 2x with 2% HNO₃ (67%–70%, Optima Grade, Fisher Chemical), to achieve a final concentration of 0.05 M NaHCO₃. Calibration was performed using solutions prepared by serial dilution of standards (Inorganic Ventures) with 2% HNO₃.

Electrochemical cell apparatus.—A custom-made glass electrochemical cell (section S3, SI) and a Au mesh counter electrode were employed in all electrochemical measurements. The Au counter electrode was fabricated by spot welding Au mesh (99.99%, 100 mesh, 25 × 25 mm, Fisher) to Au wire (99.999%, 0.762 mm diameter, 10 cm long, Fisher) using molybdenum spot welding tips (Miyachi Unitek). The counter electrode was separated from the main cell compartment by a fritted glass tube (12 mm dia., porosity D frit, Ace Glass). A reversible hydrogen electrode (RHE) was assembled using a coiled Pt wire and Luggin capillary (Fig. S2, SI) and used in 0.1 M H₂SO₄ for electropolishing. A commercial double junction Ag/AgCl reference electrode (glass body, Fisherbrand accumet or Pine Research) was filled with 4 M KCl saturated with AgCl in the inner chamber and 0.1 M NaHCO₃ in the outer chamber. The double junction electrode was selected to mitigate trace Ag⁺ leakage and used in 0.1 M NaHCO₃.³⁹ The potential difference between the Ag/AgCl/KCl (sat.)/0.1 M NaHCO₃ reference electrode and an RHE was checked before each experiment in CO₂ sat. 0.1 M NaHCO₃ by the method of Zeledón et al.⁴⁰ (Section S4, SI). Potentials were converted to the RHE scale using Eq. 1:

$$E_{RHE} = E_{Ag/AgCl(sat.KCl)} + 0.059 * pH + E_{Ag/AgCl(sat.KCl)}^0 \quad [1]$$

where $E_{Ag/AgCl(sat.KCl)}^0 = 0.197$ V. Before each experiment, the electrolyte was purged with the necessary gas to expel dissolved O₂ and saturate the solution with the purge gas. The same gas was used to either purge or blanket the headspace during the subsequent measurements. When not in use, the glassware, Au counter electrodes, and PTFE components (stopcock and stoppers) were stored in DI water to maintain cleanliness.

Electrolyte resistance compensation.—All electrochemical measurements were performed with ohmic drop compensation, typically at 85%. In some cases, potentiostat oscillation was observed at 85% compensation, so the percentage was lowered to maintain stable potentiostat operation (as indicated in the figure captions or labels). The solution resistance, R_{soln}, was measured by first performing

electrochemical impedance spectroscopy (EIS) using the parameters in section S5, SI. The EIS spectra were fit to an equivalent circuit with a resistor and constant phase element in series (R_{soln}Q circuit) to determine R_{soln}. The value of R_{soln} was measured and updated when any of the following variables changed: electrolyte composition, purge gas, working electrode area, or position of the electrodes.

Electrolyte preparation.—0.1 M NaHCO₃ solutions of varying purity were prepared using the methods of Wuttig and Surendranath.²⁷ In summary, NaHCO₃ electrolytes were either used without purification, pre-electrolyzed, or treated with Chelex resin. Pre-electrolysis was performed in a 2-electrode cell with N₂ sat. 0.1 M NaHCO₃ and Au mesh working and counter electrodes. 20 mA of current (ca. 3.0 mA cm⁻²) was applied between the electrodes for 19 h to plate trace metal electrolyte contaminants onto the Au mesh cathode. The cathode was removed from the electrolyte under cathodic polarization to prevent re-dissolution of plated impurities. The same pre-electrolysis cell was used for subsequent CO₂RR experiment to avoid transferring the pre-electrolyzed electrolyte to a new vessel. Chelex purification was performed by adding 5 g of as-received Chelex resin for every 100 ml of electrolyte. The resin was gently stirred for 24 h then filtered from the solution using a syringe filter (0.2 μm Nylon, Acrodisc) or by vacuum filtration through a membrane (0.2 μm Nylon, Cole-Parmer). Higher purity 0.1 M NaHCO₃ was prepared by combining trace metal grade Na₂CO₃ (≥99.999%) with DI water to make 0.05 M Na₂CO₃. This solution was purged with CO₂ until it reached pH_{bulk} = 6.8, indicating conversion to 0.1 M NaHCO₃.

Electrode preparation.—Poly-Au RDE and RRDE surfaces were prepared using the procedure of Goyal et al.¹⁴ with modifications. Before every experiment, electrodes were mechanically polished using diamond polishing suspension (3, 1, and 0.25 μm, MetaDi Supreme Polycrystalline, Buehler) on a MicroCloth (dia. = 7.3 cm, Buehler) affixed to a Metaserv 250 automatic polisher (Buehler). Diamond polishing suspension was specifically used to avoid enhancement of HER on Au, which can occur with alumina polish.⁴¹ For each suspension size, electrodes were polished by moving the electrode surface across the MicroCloth with moderate pressure at 400 rpm until a uniform surface finish was achieved (ca. 2–3 min). The DI water and the diamond suspension were re-applied to the MicroCloth as needed to keep the polishing cloth wet. The electrodes were then sonicated in acetone and then DI water for 5 min each prior to polishing with the next smaller suspension size or to conclude the mechanical polishing procedure. The electrode surfaces were then chemically treated by soaking in 20 wt% HNO₃ for 15 min to remove any trace metal deposits from previous experiments (Fig. S4, SI). This was followed by sonication in DI water for 20 min, refreshing the DI water once after 10 min of sonication. When not conducting polishing or experiments, the electrode surface was always covered with a droplet of DI water to prevent contamination from the ambient air.

The poly-dopamine coating procedure reported by Vos and Koper⁴² was used on RRDEs to increase the hydrophilicity of the PEEK spacer (Fig. S5, SI) and prevent gas bubble attachment between the disk and ring. The coating solution consisted of 2 g l⁻¹ dopamine HCl, 10 mM Na₂HPO₄, and 10 mM NaH₂PO₄·H₂O in DI water (pH ≈ 7). The RRDE tip was rotated at 400 rpm for 2 h in the coating solution then rinsed thoroughly with DI water. Dopamine HCl was stored at 2 °C–8 °C; however, we found that allowing the solution resulted in a coating more effective at preventing bubble attachment. The poly-dopamine coating was removed from the Au surfaces by electrochemical polishing in N₂ sat. 0.1 M H₂SO₄.¹⁴ The disk and ring were shorted together and cycled between 0.05 V and 1.75 V vs RHE for 400 cycles at a scan rate, v , of 1 V s⁻¹ (Fig. S8, SI). Next, cyclic voltammetry (CV) of the same potential region (0.05 to 1.75 V vs RHE) was performed at $v = 50$ mV s⁻¹ for the

shorted ring and disk as well as the disk alone. Both CVs were compared to the CV of an unmodified Au RRDE to ensure the dopamine coating was completely removed from the Au surfaces (Fig. S9, SI). The CVs were all performed without rotation (i.e. $\omega = 0$ rpm). The Au disk's electrochemically active surface area (ECSA) was determined by fitting the Au reduction peak with a Gaussian peak shape in the potentiostat software to calculate the charge passed during the reduction, Q_{red} . Dividing Q_{red} by the specific charge of one monolayer of gold ($390 \mu\text{C cm}^{-2}$) gave the electrochemically active surface area (ECSA) of the disk electrode.^{14,43} Unless otherwise noted, all current densities reported in this work are normalized by the disk's ECSA. The same electrochemical polishing procedure was performed on RDEs; however, RDEs were not coated with poly-dopamine.

HOR and COOR measurements.—Quantifying the FEs of Au by RRDE relies on the negligible HOR activity of Au (section S8, SI) and holding the Au ring at an oxidizing potential where the COOR is mass transport limited (section S9, SI). Au activity for HOR and CO oxidation were determined by RDE measurements based on the procedure of Goyal et al.¹⁴ in 0.1 M NaHCO₃ electrolyte of different purities. For HOR experiments, the electrolyte was purged with H₂ gas for ≥ 20 min. Afterwards, CV cycles (25 mV s^{-1}) were performed between 0.4 and 1 V vs RHE. For CO oxidation experiments, the electrolyte was sparged with CO gas for ≥ 20 min. Then, CV cycles (25 mV s^{-1}) were performed between 0.2 and 1.3 V vs RHE. Similarly, CA measurements were used to assess the activity and stability of HOR and COOR on poly-Au RDEs under the same conditions, except the RDE potential was held at a fixed value (1 V vs RHE) instead of cycled.

Plating and stripping experiments.—Trace metals in electrolytes of different purity were identified by plating and stripping experiments with Au RDEs.²⁷ Measurements were performed without iR compensation on a Au RDE in CO₂ sat. 0.1 M NaHCO₃ ($\text{pH}_{\text{bulk}} = 6.8$) at 2500 rpm. CA was performed on the Au RDE at 1 V or -0.9 V vs RHE for 5 or 45 min. Then, the Au RDE was immediately cycled between -0.2 and 1.75 V vs RHE at 50 mV s^{-1} for 10 cycles to strip metals that were plated during CA. All measurements were completed on the same electrode in a single experiment. Long duration CA experiments were also performed on RDEs to accumulate trace metal impurities from the electrolyte and detect them by subsequent XPS. For CO₂RR, a ChangeDisk Au RDE was held at -1 V for 4 h in CO₂ sat. 0.1 M NaHCO₃ ($\text{pH}_{\text{bulk}} = 6.8$) at 2500 rpm with 85% iR compensation. The cathode was removed from the electrolyte under cathodic polarization to prevent re-dissolution of plated impurities, rinsed gently with DI water, and dried under ambient laboratory conditions before XPS analysis. The same procedure was applied for long duration COOR experiments by holding at ChangeDisk Au RDE at 1 V vs RHE for 4 h in CO sat. 0.1 M NaHCO₃ ($\text{pH}_{\text{bulk}} = 9$) at 2500 rpm with 85% iR compensation. For COOR experiments, the RDE was removed from the electrolyte under anodic polarization.

RRDE CO₂RR selectivity measurements.—After properly polishing the RRDE, coating with poly-dopamine, electropolishing and characterizing the RRDE in H₂SO₄, and calibrating the reference electrode, the RRDE tip was transferred to a clean electrochemical cell for FE_{CO} selectivity measurements. 0.1 M NaHCO₃ of different purities was sparged with CO₂ gas for ≥ 20 min until $\text{pH}_{\text{bulk}} = 6.8$. Next, the purity of the electrolyte was evaluated by the method of Cui et al.²⁶ by cycling the disk between 0.65 and -0.60 V_{RHE} at 50 mV s^{-1} under forced convection and observing the percentage change in current density at -1.6 V vs RHE (section S10, SI). CV experiments were performed by cycling the disk electrode between 1.75 V and -1 V vs RHE at 25 mV s^{-1} while the ring electrode was held at 1 V vs RHE. CA experiments were performed by holding the disk electrode at the desired reducing potential (in range of -0.4 to -1.0 V vs RHE) and the ring electrode at 1 V vs RHE for 5 min.

Unless otherwise noted, measurements always started with the least negative cathodic potential and proceeded to more negative potentials. After each CV or CA measurement, the RRDE was cleaned by shorting the ring and disk electrodes then cycling at 2500 rpm between 0.05 and 1.75 V vs RHE at 25 mV s^{-1} for 10 cycles. The collection efficiency of the RRDE was experimentally determined using the Fe(CN)₆³⁻/Fe(CN)₆⁴⁻ redox couple after all CV and/or CA measurements were completed. The electrolyte was sparged with N₂ for ≥ 50 min until $\text{pH}_{\text{bulk}} = 9$, and 5 mM K₃Fe(CN)₆ was dissolved in the electrolyte. Next, the disk electrode was cycled between 1.3 and 0.28 V vs RHE at 25 mV s^{-1} for each rotation rate used in the previous CV and/or CA measurements while the ring electrode was held at 1.13 V vs RHE. The mass transport limited ring and disk currents, i_L , were determined by fitting the data to a sigmoid function (Eq. 2):

$$i = \frac{i_L}{1 + e^{-k(E_{\text{disk}} - x_0)}} + b \quad [2]$$

where i and E_{disk} are the experimentally measured current (ring or disk) and disk potential, respectively. The mass transport limited current is given by i_L . k , x_0 , and b are fitting constants. The collection efficiency, N , is then calculated from the ratio of $i_{L,\text{ring}}$ and $i_{L,\text{disk}}$ and the number of electrons transferred in the disk and ring reactions ($n_D = 1$ and $n_R = 1$) (Eq. 3):

$$N = \left| \left(\frac{i_{L,\text{ring}}}{i_{L,\text{disk}}} \right) \left(\frac{n_D}{n_R} \right) \right| \quad [3]$$

Examples of the experimental CV, fitting results, and collection efficiency values are provided in section S11, SI. Calculations for the CO and H₂ partial current densities (j_{CO} and j_{H_2}) and faradaic efficiencies (FE_{CO} and FE_{H₂}) were carried out by the subtraction method reported by Goyal et al. and outlined by Eqs. 4–7.¹⁴

$$j_{\text{CO}} = \frac{-i_{\text{ring}}}{N \times \text{ECSA}_{\text{disk}}} \quad [4]$$

$$\text{FE}_{\text{CO}} = \frac{i_{\text{ring}} \times 100}{|i_{\text{disk}}| \times N} \quad [5]$$

$$j_{\text{H}_2} = j_{\text{disk}} - j_{\text{CO}} \quad [6]$$

$$\text{FE}_{\text{H}_2} = 100 - \text{FE}_{\text{CO}} \quad [7]$$

Plotting convention.—All current and voltage data is plotted using the IUPAC convention.

Results and Discussion

RRDE cyclic voltammetry measurements.—Our initial experiments attempted to reproduce FE_{CO} vs E_{disk} data from published literature using a poly-Au/Au RRDE and CV measurements in disk-scan mode. The experimental procedure closely follows that which was reported by Goyal et al.¹⁴ and Vos et al.¹⁸ Despite identical CO₂RR conditions (0.1 M NaHCO₃, sat. CO₂, $\text{pH}_{\text{bulk}} = 6.8$, $\omega = 2500$ rpm), we observe significantly lower selectivity toward CO production compared to Goyal et al. at all potentials in the range -0.4 to -0.8 V vs RHE (Fig. 2a). Comparison to data from Vos et al. shows closer agreement with our CV results, especially in the range $E_{\text{disk}} = -0.7$ to -1.0 V vs RHE. Note that data from Goyal et al. and Vos et al. is shown in Fig. 2a as discrete points; however, both these works used CV for FE_{CO} measurements.^{14,18} Chauhan et al. also reported FE_{CO} measurements by staircase voltammetry; however, their system used 10% CO₂/90% N₂ as the purge gas, resulting in a more alkaline electrolyte with $\text{pH}_{\text{bulk}} = 7.7$.¹⁶ Qualitatively, all four data sets display a similar trend: CO selectivity is maximized at

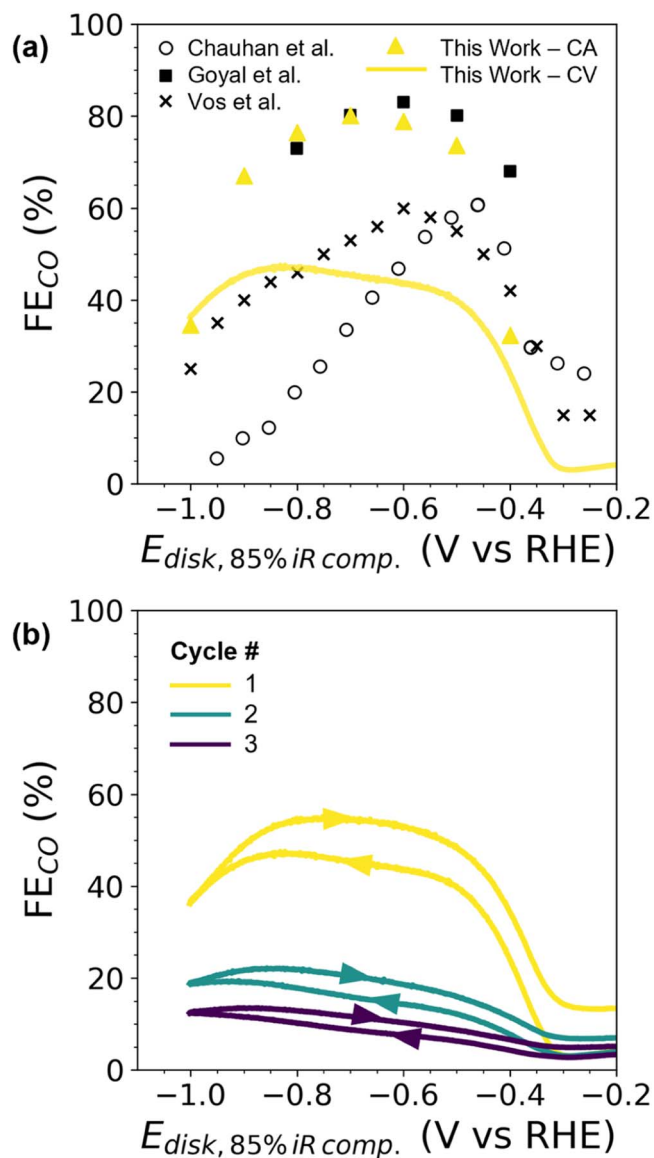


Figure 2. (a) Comparison of FE_{CO} vs E_{disk} on poly-Au/Au RRDEs between this work's CV (yellow solid line) and CA (yellow triangles) measurements to previous literature reports by Chauhan et al. (black open circles),¹⁶ Goyal et al. (black filled squares),¹⁴ and Vos et al. (black crosses).¹⁸ Chauhan et al. performed measurements in 0.1 M NaHCO_3 ($\geq 99.7\%$, 10% CO_2 sat., $\text{pH}_{\text{bulk}} \approx 7.7$, $\omega = 2500$ rpm) using staircase voltammetry. Adapted with permission from Ref. 16. Copyright 2023 American Chemical Society. Goyal et al. performed measurements in 0.1 M NaHCO_3 ($\geq 99.7\%$, CO_2 sat., $\text{pH}_{\text{bulk}} = 6.8$, $\omega = 2500$ rpm, $\nu = 25$ mV s^{-1}) using CV. Adapted from Ref. 14. Copyright 2020 American Chemical Society. Vos et al. performed measurements in 0.1 M NaHCO_3 ($\geq 99.7\%$, CO_2 sat., $\text{pH}_{\text{bulk}} = 6.8$, $\omega = 2500$ rpm, $\nu = 20$ mV s^{-1}) using CV. Adapted from Ref. 18 under terms of the CC-BY license. Copyright 2022, The Authors. ChemElectroChem published by Wiley-VCH GmbH. (b) FE_{CO} as a function of E_{disk} determined by CV from this work in 0.1 M NaHCO_3 ($\geq 99.7\%$, CO_2 sat., $\text{pH}_{\text{bulk}} = 6.8$, $\omega = 2500$ rpm, $\nu = 25$ mV s^{-1}) on a poly-Au/Au RRDE. Colored arrows along the solid lines indicate the CV scan direction.

intermediate reducing potentials but suppressed at the upper and lower ends of the measured potential region. The bell-shaped FE_{CO} vs E_{disk} plot has been attributed to changes in the primary proton donor for the HER from H_2CO_3 to HCO_3^- to H_2O as E_{disk} becomes more negative.¹⁵ However, the four data sets are *quantitatively* quite dissimilar. For example, the maximum FE_{CO} and potential where it occurs are very different: 55% at -0.75 V for this work, 83% at -0.6 V for Goyal et al., and 60% at -0.46 V for Chauhan et al.

Figure 2a also shows that FE_{CO} is highly dependent on the electrochemical method. FE_{CO} measurements using CA instead of CV gave a maximum FE_{CO} of 80% at -0.7 V which is nearly 20% higher than the CV measurement at the same disk potential. Further discussion of the CA data is given in the “RRDE chronoamperometry measurements” section. It is necessary to determine the causes of these discrepancies before results can be reliably compared across laboratories.

Figure 2b shows the dependence of FE_{CO} on the scan direction and cycle number of the CV in this work. First, the reverse scan always measures a higher FE_{CO} than the forward scan at all measured potentials. We hypothesize this hysteresis is due to an interfacial pH effect where at the same potential, the pH at the electrode surface is more alkaline on the forward sweep than the reverse sweep, as shown by Liu et al.²² However, other possible explanations could include accumulation of cations at the electrode surface to stabilize CO_2RR intermediates or suppression of adsorbed H by competition with adsorbed CO.^{44,45} Second, as the cycle number increases there is a dramatic decrease in FE_{CO} . For example, the selectivity for CO between the forward scans of cycle 1 and 3 at -0.6 V vs RHE decreases by 36%, demonstrating poor measurement stability despite a relatively short (11 min) CV experiment. This phenomenon has not been previously reported in Au/Au RRDE studies yet was consistently observed in our results when conducting CV measurements over multiple cycles in a variety of electrolytes (section S12, SI). Deactivation of poly-Au electrodes for CO_2RR is well-documented^{27,28,36} but has not been thoroughly investigated in the context of selectivity measurements by RRDE. Some works have noted the need to “condition” or “reactivate” the RRDE after cathodic polarization by cycling the ring and disk electrodes anodically in the Au oxidation/reduction region but did not elaborate further.^{16,26,42}

To date, Cui et al. have provided the most rigorous analysis of Au deactivation during RRDE studies by focusing on trace metal impurities from electrolyte reagents.²⁶ The authors found that high purity reagents treated with Chelex to remove trace metals resulted in the highest FE_{CO} . They also proposed a method for determining the purity of NaHCO_3 electrolytes: “ $<5\%$ change in electrocatalytic activity at -0.6 V_{RHE} after 10 cycles of potential cycling between 0.65 and -0.60 V_{RHE} at 50 mV s^{-1} under forced convection, can be used as a benchmark for minimum electrolyte purity.” This is a useful benchmark for evaluating electrolyte purity; however, it relies on changes in j_{disk} and therefore is not a direct evaluation of FE_{CO} deactivation. Furthermore, CV experiments will convolute the effects of a changing electrode potential with deactivation processes, making it difficult to determine which variable is affecting FE_{CO} during the potential sweep. This raises the concern that if deactivation mechanisms are not detected in a CV, they could lead to inaccurate mechanistic conclusions.

RRDE chronoamperometry measurements.—To decouple the effect of changing potentials and deactivation over time, we performed CA measurements at a fixed disk potential of -0.65 V vs RHE for 5 min (Fig. 3a). Like in the CV measurements, FE_{CO} decreases rapidly from 80% to 24% between 30 s and 5 min. We do not consider the first 30 s to avoid contributions from non-Faradaic double layer charging currents to the calculated FE_{CO} values. To reactivate the electrode, the ring and disk were shorted together and cycled 10 times from 0.05 to 1.75 V vs RHE before the next CA hold (Fig. 3b). This anodic cycling method recovers the initial selectivity of the Au electrode for CO (Fig. 3a) but does not prevent deactivation upon subsequent cathodic polarization. The mechanism of Au reactivation by anodic cycling is discussed in a later section.

The reactivation CV (Fig. 3b) shows the normal redox features of Au oxidation and reduction.^{28,46} The onset of the oxygen evolution reaction (OER) is also observed ca. 1.75 V vs RHE which causes in situ O_2 generation. This O_2 is detected in subsequent CV sweeps as a cathodic oxygen reduction reaction (ORR) current (ca. <0.6 V vs RHE) that increases in magnitude with each subsequent CV cycle

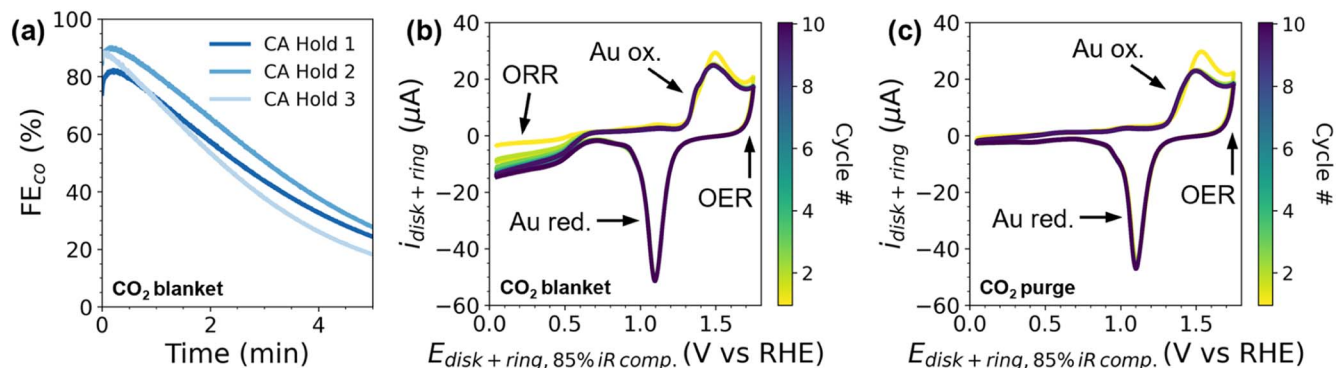


Figure 3. (a) FE_{CO} as a function of time on a poly-Au/Au RRDE in 0.1 M NaHCO_3 ($\geq 99.7\%$, CO_2 sat., $\text{pH} = 6.8$) with $E_{\text{disk}} = -0.65$ V vs RHE, $E_{\text{ring}} = 1$ V vs RHE, and $\omega = 2500$ rpm. Three CA holds were performed sequentially on the same electrode with anodic reactivation CVs between each CA measurement to reactivate the electrode. (b)–(c) Representative electrode reactivation CVs in 0.1 M NaHCO_3 ($\geq 99.7\%$, CO_2 sat., $\text{pH}_{\text{bulk}} = 6.8$) with the electrolyte either (b) blanketed with CO_2 or (c) purged with CO_2 .

as more O_2 is produced: the current at 0.05 V vs RHE increases from -3.5 μA to -14.6 μA over 10 reactivation cycles (Fig. 3b).

The presence of O_2 in the electrolyte is undesirable for FE_{CO} measurements because the resulting ORR current will contribute to the measured j_{disk} and calculated j_{H_2} . The subtraction method for calculating FEs assumes that the Au disk only produces CO and H_2 as products, so any disk current not attributed to CO production is assigned to j_{H_2} (see Eq. 6). However, the ORR current can be largely eliminated by continuously purging the electrolyte with CO_2 throughout the experiment (Fig. 3c) instead of blanketing the electrolyte with CO_2 . In this configuration, the CO_2 gas is purged into the electrolyte far enough away from the RRDE to prevent bubble attachment or altering the fluid flow pattern near the electrode surface. The ORR current at 0.05 V vs RHE reaches at most -2.8 μA over 10 reactivation cycles with constant CO_2 purging, a significant decrease compared to the -14.6 μA measured when the electrolyte is simply blanketed by CO_2 .

Effect of O_2 on FE_{CO} measurements.—The effects of dissolved O_2 and ORR on quantitative FE_{CO} measurements were determined by conducting additional CA measurements in 100 mV increments from $E_{\text{disk}} = -0.4$ to -1 V vs RHE. Results were compared between a cell blanketed by CO_2 and a cell continuously purged by CO_2 . Representative FE_{CO} vs time plots are shown in Fig. S25, SI, which show clear differences in the maximum FE_{CO} at each potential and the deactivation rate, i.e. the slope. Reactivation CVs were performed after each CA hold, and the effectiveness of CO_2 purging for expelling O_2 is evidenced by the minimal ORR current compared to a cell that was blanketed by CO_2 (Figs. S26 and S27, SI).

Figure 4 summarizes FE_{CO} , j_{CO} , and j_{H_2} data for both cases at 30 s and 5 min of the CA experiment. At 30 s, FE_{CO} is within error at all potentials more cathodic than -0.4 V when comparing the CO_2 blanketed and purged cases (Fig. 4a). However, at -0.4 V, FE_{CO} is significantly higher in the CO_2 purged case (64%) than the CO_2 blanket case (32%). At low reduction overpotentials where j_{disk} is small, the current from ORR accounts for a significant percentage of the overall disk current. The ORR current contributes to the calculated partial current density for HER, j_{H_2} , thereby artificially increasing the electrode's selectivity toward H_2 . As the reduction overpotential increases, j_{disk} grows exponentially and therefore any ORR current is insignificant compared to j_{CO} and j_{H_2} .

A more substantial effect on FE_{CO} is observed at 5 min after the electrode has noticeably deactivated (Fig. 4d). FE_{CO} is consistently lower than FE_{H_2} at all potentials ≤ -0.5 V vs RHE when CO_2 is purged into the electrolyte. Correspondingly, j_{CO} and j_{H_2} are also lower and higher, respectively. Clearly, the Au electrode deactivates more rapidly in the presence of CO_2 purging. It is unlikely this accelerated deactivation is still a result of enhanced O_2 removal by constant purging: FE_{CO} at -0.4 V at 5 min for both cases are nearly

identical (ca. 11%), indicating the majority of dissolved O_2 has been consumed by ORR after 5 min of cathodic reduction. If significant quantities of O_2 were still present at 5 min, the data should resemble the result at 30 s where FE_{CO} is reduced in the CO_2 blanket case because ORR contributes to the calculated j_{H_2} .

We suspect a difference in the bulk pH between the CO_2 blanketed and purged electrolytes could explain the FE_{CO} trend at 5 min. During a CA experiment, the CO_2 reactant is continuously consumed. Constant purging of the electrolyte with CO_2 replenishes the CO_2 consumed by the reaction and maintains the bulk pH at 6.8. If the electrolyte is only blanketed by CO_2 , the diffusion between the gas headspace and electrolyte is too slow to replenish the CO_2 , leading to a gradual increase in bulk pH. Alkaline conditions are known to favor CO_2RR over HER,^{47,48} which would explain why the blanketed electrolyte shows higher FE_{CO} than the purged electrolyte. Loboccaro et al. also noted the effect of CO_2 mass transport on bulk pH over long studies: the pH of 0.1 M NaHCO_3 increased by 0.15 pH units after just 1 h of CO_2RR at a 7.5 mA cm^{-2} .⁴⁹ The authors found that purging the electrolyte with smaller, high surface area CO_2 bubbles prevented gradual alkalization of the bulk electrolyte up to 15 mA cm^{-2} . However, a robust investigation of this hypothesis is outside the scope of this article. For the remainder of this work, the electrochemical cell was constantly purged with CO_2 to remove O_2 , minimize ORR contributions to j_{disk} and j_{H_2} , and replenish consumed CO_2 .

Relative contributions of disk and ring to deactivation.—RRDE selectivity measurements rely on both CO_2RR at the disk and COOR at the ring. Deactivation of either reaction would cause an apparent decrease in FE_{CO} during CA measurements. Figure 5 presents a sequence of CA and reactivation CV measurements to determine the relative contribution of the disk and ring reactions to overall deactivation (see also section S14, SI). First, a freshly prepared poly-Au RRDE was reactivated with the ring and disk electrodes shorted together. Next, a CA measurement recorded FE_{CO} deactivation over 5 min of CO_2RR (Fig. 5a) decreasing from 81% at 30 s to 7% at 5 min. This process was repeated with only reactivating either the disk or the ring electrode. Subsequent CAs showed neither case fully recovered the initial CO selectivity (Figs. 5b, 5d). When only the disk is reactivated, the FE_{CO} does not recover at all: 2% after 30 s of CA (Fig. 5b). When only the ring is reactivated, FE_{CO} partially recovers to 59% after 30 s of CA but gradually decreases to 5% after 5 min. However, the electrode can always be fully reactivated by simply electronically shorting the ring and disk together and applying the reactivation CV to recover initially high (i.e. $>80\%$) CO selectivity (Figs. 5c, 5e). Thus, we conclude that both the ring and disk contribute to the observed FE_{CO} deactivation.

Figure 5d also suggests that disk deactivation accounts for a nearly 30% FE_{CO} decrease after 30 s of CA. This was determined by

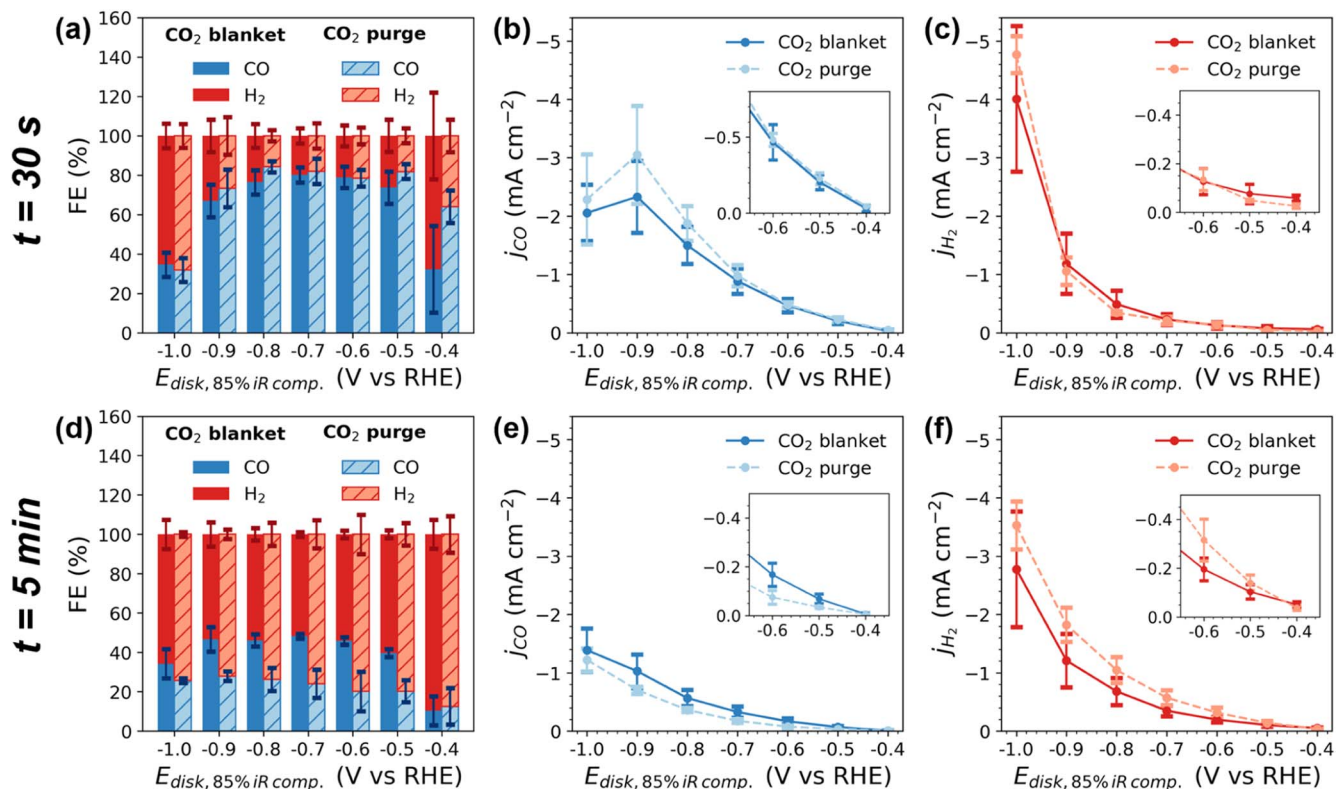


Figure 4. Selectivity (a), (d), j_{CO} (b), (e), and j_{H_2} (c), (f) results from CA experiments at 30 s (a)–(c) and 5 min (d)–(f) on a poly-Au/Au RRDE. E_{disk} was held for 5 min at potentials from -0.4 to -1 V vs RHE in 100 mV increments. The electrolyte was either blanketed or purged with CO₂ as indicated. Between each potential hold, the ring and disk were shorted together and cycled 10 times between 0.05 and 1.75 V vs RHE to reactivate the RRDE. All experiments were performed in 0.1 M NaHCO₃ ($\geq 99.7\%$, CO₂ sat., $pH_{bulk} = 6.8$) with $E_{ring} = 1$ V vs RHE, $\omega = 2500$ rpm, and $v = 25$ mV s⁻¹. Error bars indicate the standard deviation of $n = 3$ independent measurements on a freshly prepared electrode. Selectivity data represent instantaneous measurements at 30 s and 5 min in panels (a) and (d), respectively. Lines in panels (b, c) and (e, f) are meant to guide the eye.

comparing the FE_{CO} at 30 s after reactivation of *both* disk and ring (Fig. 5c) to FE_{CO} at 30 s after reactivation of the ring only (Fig. 5d). In the latter case, the ring has been reactivated, so the difference in FE_{CO} between the two cases (88% vs 59%) must be attributed to failure of CO production at the disk electrode. This suggests that the remaining $\sim 60\%$ of FE_{CO} deactivation is due to COOR deactivation at the ring electrode. Additional RDE measurements in CO sat. 0.1 M NaHCO₃ ($\geq 99.7\%$) confirmed that the COOR is unstable on poly-Au over 5 min of CA (Figs. S14a and S16a, SI) but can be reactivated by the anodic cycling treatment.

It is important to note that the mechanisms causing deactivation of CO₂ reduction to CO at the disk or CO oxidation at the ring are not necessarily the same. In fact, the reactivation CVs of the disk (Fig. 5g) and ring (Fig. 5h) are distinctly different in the first cycle, further supporting that the deactivation mechanisms are different. Specifically, the disk's reactivation CV exhibits a small, broad peak at ~ 0.9 V vs RHE and increased current at 1.75 V vs RHE on the first cycle. Conversely, the ring's reactivation CV displays only an increase and positive potential shift of the Au oxidation peak at ~ 1.5 V vs RHE. After 10 cycles, these features disappear completely, and the final reactivation CV cycle of the ring or disk appear identical. The remainder of this work focuses on identifying the deactivation mechanisms affecting the ring and disk electrodes.

Identification and stripping of trace metal impurities.—One of the most common culprits for CO₂RR deactivation identified in literature is the plating of trace metal contaminants from the electrolyte. Several works have identified Cu, Zn, Pb, and Fe as the main contaminants from sodium bicarbonates, even with reagents exceeding 99.999% in purity.^{26–28}

To identify trace metals in our system, CVs were performed on a poly-Au RDE immediately after 5 min or 45 min CA at 1 V or

-0.9 V vs RHE. These potentials were chosen to represent the ring and disk potentials during a typical RRDE selectivity measurement. Figure 6 highlights the stripping features, and plots of the complete CV range (-0.2 to 1.75 V vs RHE) are given in section S15, SI. The sloping background cathodic current observed in all CVs is likely a result of ORR from in situ generated O₂ during stripping experiments.

As expected, the CA holds at 1 V vs RHE do not result in new stripping features (Figs. 6b, 6d) compared to the clean Au RDE (Fig. 6a) since it is unlikely trace metals will deposit at this oxidizing potential. In the case of a CA hold at -0.9 V vs RHE, several new stripping peaks are observed, which grow as the electrolysis time is increased from 5 min to 45 min. The peaks at -0.08 and 0.08 V vs RHE correspond well to previous reports of Zn⁰ stripping from Au.²⁷ The broad stripping peak at more positive potentials (ca. 0.75 to 1.20 V) is typically assigned to stripping of Cu species.^{27,28} The identity of the sharp oxidation and reduction peaks at ca. 0.5 V vs RHE has been debated despite being observed repeatedly in studies of sodium bicarbonate electrolyte purity.^{26,27} Wuttig and Surendranath assigned the peak to Cu stripping at 0.56 V vs RHE.²⁷ Conversely, Cui et al. suggested this peak is a convolution of Pb stripping, Pb underpotential deposition, and electrochemical lifting of Au surface reconstruction, which occur in the range 0.20 to 0.80 V vs RHE.²⁶ Our results closely align with those of Cui et al. in the position of the peaks, their gradual decrease in area with increased cycling, and their shift to higher potentials. We also observe the same effects on the Au redox features with repeated stripping cycles: a reduction and negative shift in the Au oxidation peak and increase and positive shift in the Au reduction peak. Notably, this peak also appears in the CVs of the freshly prepared RDE and after CA at 1 V vs RHE, again suggesting it may not solely be due to trace metal deposition.

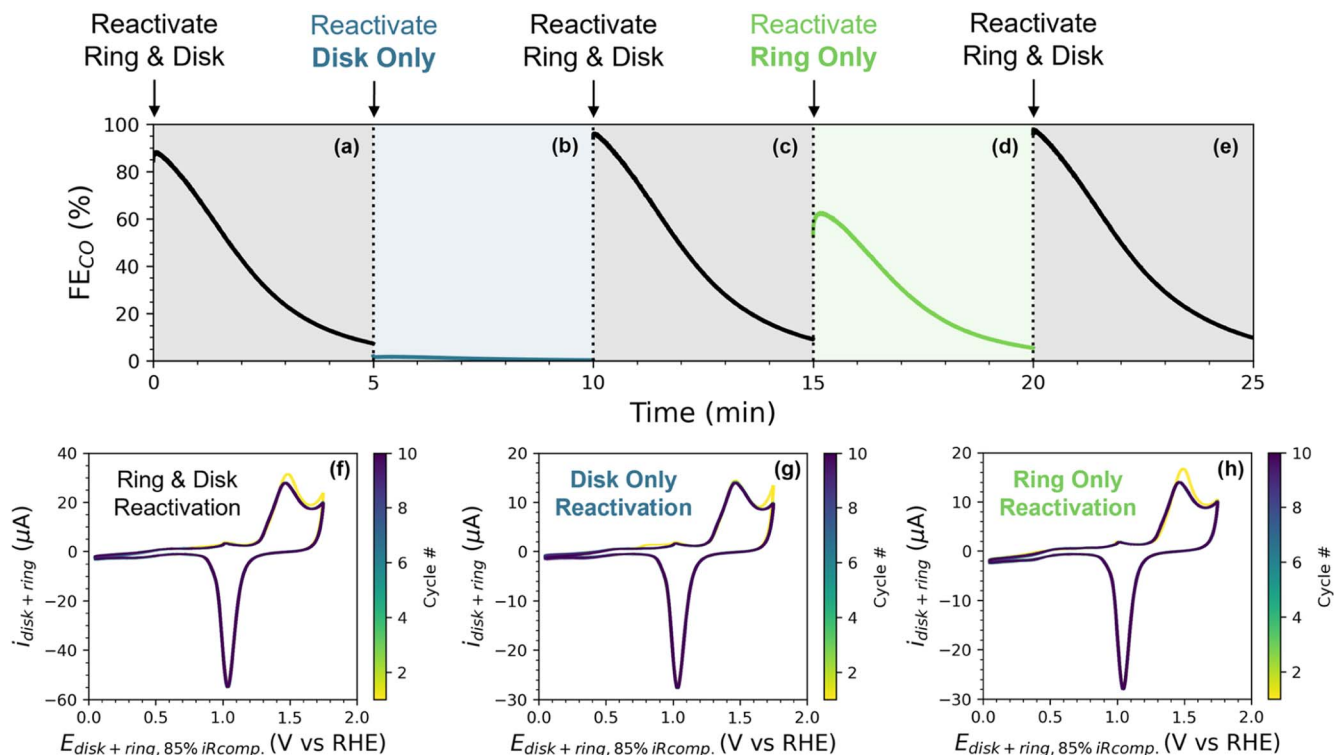


Figure 5. FE_{CO} selectivity data collected from a sequence of five CA measurements with $E_{\text{disk}} = -0.6$ V vs RHE and $E_{\text{ring}} = 1$ V vs RHE (a)–(e). Before each 5 min CA hold, 10 reactivation CV cycles were performed between 0.05 and 1.75 V vs RHE at $v = 25$ mV s⁻¹ as indicated by the arrows at the top of the figure. CA was performed after reactivating both the disk and ring (a), (c), (e), the disk only (b), or the ring only (d). Representative reactivation CVs of both the disk and ring (f), the disk only (g) or the ring only (h). Note the difference in current axis scaling among panels (f)–(h). All experiments were performed in 0.1 M NaHCO₃ ($\geq 99.7\%$, CO₂ sat., pH_{bulk} = 6.8) with $\omega = 2500$ rpm and continuous CO₂ purging.

The stripping results in Fig. 6 also explain why the reactivation CVs (Figs. 3b, 3c) effectively recover the Au electrode's selectivity for CO. Several previous works have used anodic treatments including cyclic voltammetry,^{28,36} open-circuit holds,²⁸ and anodic pulsing⁵⁰ to reactivate Au electrodes for CO₂RR. All these methods work by electrochemically stripping trace metal contaminants and organic poisons from the electrode surface. Anodic reactivation, however, has been criticized for inducing restructuring, roughening, and/or dissolution of the Au electrode.³⁶ However, this system does not show evidence of restructuring from anodic cycling treatments. Firstly, the reactivation CVs are consistent across multiple anodic cycles (Fig. S27, SI) with no change in the Au reduction peak area. Secondly, the FE_{CO} vs time plot (Fig. 2a) is reproducible within $\sim 10\%$ after repeated CA and reactivation experiments.

Further measurements by XPS before and after 4 h of CO₂RR in CO₂ sat. 0.1 M NaHCO₃ ($\geq 99.7\%$) confirmed the chemical identity of the trace metals as Zn, Cu, Fe, and Pb (section S17, SI). XPS was also used to confirm that the polishing protocols would prevent trace metal deposits from carrying over on Au electrodes from previous experiments (Fig. S4, SI). Zn and Pb were effectively removed by mechanical polishing with diamond slurry, but, surprisingly, Cu persisted on the surface. Additional chemical treatment of the Au electrode by soaking in 20 wt% HNO₃ was necessary to remove the Cu contaminants, and thus this was added to our electrode preparation procedure for all experiments.

XPS measurements were also performed after 4 h of COOR in CO sat. 0.1 M NaHCO₃ ($\geq 99.7\%$) on a poly-Au RDE to investigate the deposition or adsorption of electrolyte impurities under the same experimental conditions experienced by the RRDE's ring electrode (section S18, SI). Significant amounts of Ag (>9 at%) were found on the RDE surface after COOR in addition to lesser quantities of I (Fig. S44, SI). Zn, Cu, Fe, and Pb were not detected.

Effect of electrolyte purity on deactivation rates.—Clearly, trace electrolyte impurities are present and will deposit on the disk and ring electrodes under the conditions of an RRDE selectivity measurement. Deposition of metals on the poly-Au disk is expected to alter its selectivity over time as more trace metals accumulate on the surface. Zn has similar CO₂RR selectivity to Au but produces more formate in addition to CO. Cu deposits will produce more H₂ and a variety of CO₂RR reduction products (methane, ethylene, ethanol, and formate) compared to Au. Pb and Fe produce almost entirely formate and H₂, respectively.⁴ Accumulation of Ag or I⁻ onto the ring electrode would both be expected to reduce electrocatalytic activity for CO oxidation. Ag is considered largely inactive for the COOR in base, and I⁻ has been shown to totally deactivate the COOR on Au particles.^{51,52}

To isolate the effect of trace impurities from other possible deactivation mechanisms, RRDE CV experiments were repeated in electrolytes with differing purities ($\geq 99.7\%$, $\geq 99.999\%$) or purification treatments (pre-electrolysis, Chelex purification) (section S12, SI). For each electrolyte, we discuss the effects of electrolyte purity on the deactivation of both CO₂RR and COOR at the disk and ring electrodes, respectively.

Pre-electrolyzing 0.1 M NaHCO₃ ($\geq 99.7\%$) resulted in a maximum FE_{CO} of 43% at -0.76 V vs RHE with clear deactivation upon repeated cycling (Fig. S20, SI). These results offer no improvement in FE_{CO} or stability compared to CVs in unpurified 0.1 M NaHCO₃ ($\geq 99.7\%$) (Figs. 2; S19, SI), indicating that pre-electrolysis does not effectively reduce deactivation for this particular electrolyte and purity. The CVs in pre-electrolyzed electrolyte also exhibited significant noise in the *i*_{disk} and *i*_{ring} measurements which were caused by the formation of high surface area Au deposits during CO₂RR that were poorly adhered to the RRDE surface (Fig. S21, SI). These Au deposits likely arise from dissolution of the Au mesh

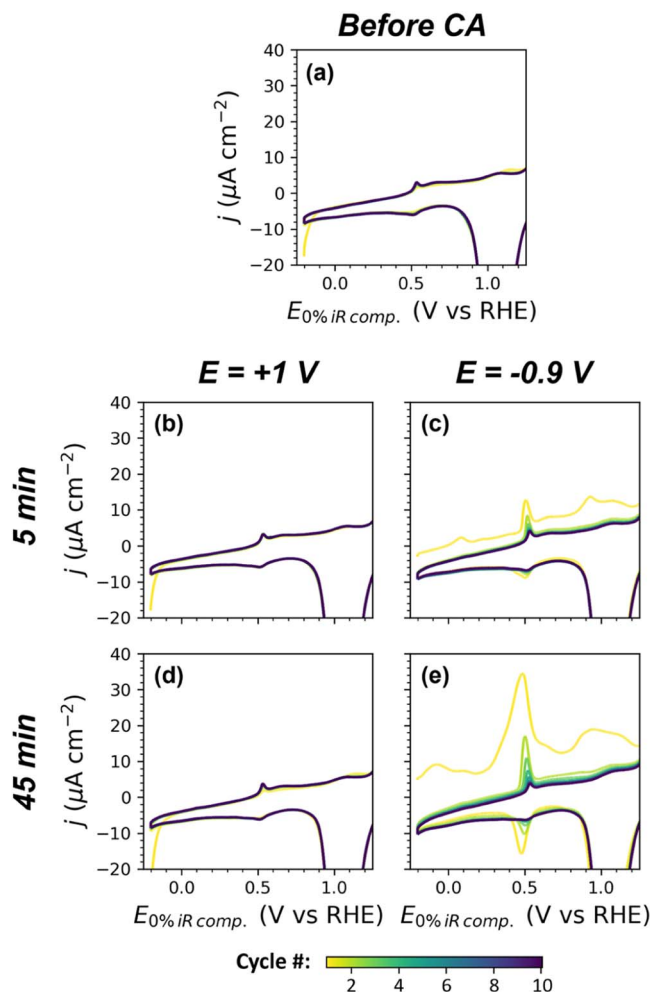


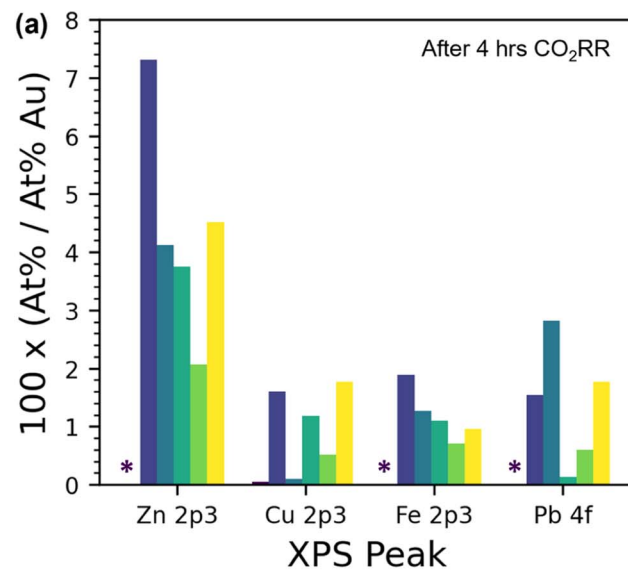
Figure 6. CVs recorded on a poly-Au RDE (a) before CA and immediately after CA at (b) +1 V for 5 min, (c) -0.9 V for 5 min, (d) +1 V for 45 min, and (e) -0.9 V for 45 min (all potentials are vs RHE). Each CV was recorded between -0.2 and 1.75 V vs RHE for 10 cycles at 50 mV s⁻¹ in untreated 0.1 M NaHCO₃ ($\geq 99.7\%$, CO₂ sat., pH_{bulk} = 6.8) at 2500 rpm. The electrolyte was continuously purged with CO₂ for all CV and CA measurements.

anode into the electrolyte during the pre-electrolysis.²⁸ ICP-MS analysis of the electrolyte before and after pre-electrolysis confirmed the Au concentration rose from 7 ppb to 679 ppb. The dissolved Au species then deposit onto the disk during subsequent CO₂RR experiments and increase the effective surface area of the electrode. Compositional analysis by XPS (Fig. 7a) of an RDE surface after 4 h of CO₂RR shows that pre-electrolysis reduced the presence of Zn, Cu, and Fe on the electrode surface compared to unpurified 0.1 M NaHCO₃ ($\geq 99.7\%$).

We also investigated the impact pre-electrolysis has on the COOR by CA and XPS. Pre-electrolysis slightly reduced the deactivation of COOR on a poly-Au RDE over 5 and 15 min of CA at 1 V vs RHE (Fig. S16b, SI). After 5 min of CA, the COOR current density in pre-electrolyzed electrolyte was 0.96 mA cm⁻² compared to 0.86 mA cm⁻² in untreated 0.1 M NaHCO₃ ($\geq 99.7\%$) electrolyte. Post-COOR XPS measurements showed that pre-electrolysis did not uniformly decrease the presence of trace impurities on the electrode surface. Notably, the surface Cu and I concentration increased while Ag decreased compared to the untreated electrolyte.

Simply switching to a higher purity commercial NaHCO₃ reagent ($\geq 99.999\%$) also reduces the presence of trace metals and increases the maximum FE_{CO} in CV experiments to 57.4% at -0.88 V vs RHE (Fig. S22, SI). We conclude that pre-electrolysis is not an effective

— After Mechanical & Chemical Polish
 — 0.1 M NaHCO₃ (99.7%)
 — 0.1 M NaHCO₃ (99.7%), pre-electrolyzed
 — 0.1 M NaHCO₃ (99.999%)
 — 0.1 M NaHCO₃ (99.999%), Chelex purified
 — 0.1 M NaHCO₃ (99.999%), H₂SO₄ cleaned glassware



— 0.1 M NaHCO₃ (99.7%)
 — 0.1 M NaHCO₃ (99.7%), pre-electrolyzed
 — 0.1 M NaHCO₃ (99.999%)
 — 0.1 M NaHCO₃ (99.999%), Chelex purified

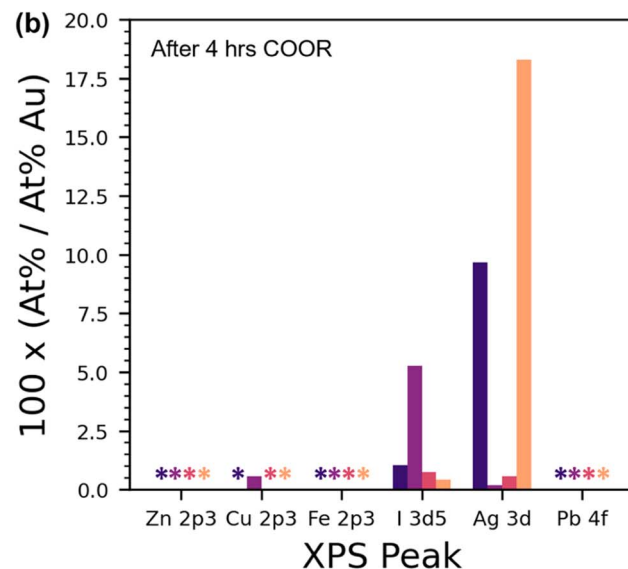


Figure 7. Selected surface composition data from XPS measurements on poly-Au RDEs after (a) 4 h of CO₂RR at -1 V vs RHE or (b) 4 h COOR at 1 V vs RHE in 0.1 M NaHCO₃ of different purities. Compositional data was normalized to the atomic percentage of Au for each sample. All glassware was cleaned by the citric acid method unless otherwise noted in the legend. Asterisks (*) indicate that the element was not detected on the RDE surface by XPS. The complete data set with and without normalization to At% Au are given in sections S17 and S18, SI.

electrolyte purification method in the context of RRDE selectivity measurements due to persistent FE_{CO} deactivation and the Au dissolution/deposition issue.

Another common purification method for bicarbonate electrolytes is pre-treatment with Chelex resin, a styrene divinylbenzene

copolymer with iminodiacetate functional groups that will bind with metal ions in solutions of $\text{pH} \geq 4$.^{26,27,53} Compositional data from XPS showed that CO_2RR in Chelex purified 0.1 M NaHCO_3 ($\geq 99.999\%$) resulted in the lowest surface concentrations of Zn, Cu, Fe, and Pb of all the electrolytes investigated (Fig. 7a), indicating that Chelex is highly effective at removing trace metal contaminants from the electrolyte. Surprisingly, this did not translate to higher FE_{CO} or decreased deactivation. In fact, CV experiments in Chelex purified electrolyte showed the lowest FE_{CO} of all electrolytes and continued deactivation with repeated cycling (Fig. S24, SI). This result is in stark contrast to previous reports, which found Chelex purification reduced trace metal contamination and improved CO selectivity on poly-Au electrodes.^{26,27} The discrepancy between our results and those of Wuttig et al.²⁷ may be due to differences in product detection methods. Wuttig et al. used gas chromatography for product analysis, whereas this work employs an electrochemical detection technique by CO oxidation at the ring electrode. We hypothesize that trace organic contamination introduced by the Chelex treatment could alter the disk's selectivity for CO or inhibit CO detection at the ring. This hypothesis is supported by CA measurements of the COOR in Chelex treated 0.1 M NaHCO_3 ($\geq 99.999\%$) that showed a rapid decrease in current density from 1.0 to 0.25 mA cm^{-2} over 5 min (Fig. S16d). In comparison, the same purity electrolyte without Chelex treatment exhibited the most stable COOR current over 5 min, dropping from 1.2 to 1.1 mA cm^{-2} over 5 min (Fig. S16c). These data indicate that Chelex treatments can have a severe impact on COOR stability. Post-COOR XPS showed a nearly 40x increase in Ag on the electrode surface when Chelex treated 0.1 M NaHCO_3 ($\geq 99.999\%$) electrolyte was used compared to untreated 0.1 M NaHCO_3 ($\geq 99.999\%$) electrolyte, suggesting that Ag impurities introduced by Chelex are also responsible for COOR deactivation. Curiously, Cui et al. employed the same RRDE product detection method used here but reported enhanced FE_{CO} in Chelex purified electrolytes.²⁶ Thus, there may be unidentified variables affecting the efficacy of Chelex purification, and further investigations are necessary. Electrochemical surface enhanced Raman spectroscopy would be a particularly useful technique to identify surface contaminants but would require Au roughening to achieve the signal enhancement effect.⁵⁴ Electrochemical atomic force microscopy or scanning tunneling microscopy can detect adsorbates on Au electrodes with molecular resolution;^{55,56} however, these techniques lack the chemical specificity of Raman spectroscopy. Thus, we expect a combination of spectroscopic and microscopic techniques would be necessary to understand the chemical nature and spatial distribution of contamination and their effects on deactivation.

Effect of glassware cleaning method on deactivation rates.—

Lastly, the effect of the glassware cleaning procedure on FE_{CO} and deactivation was determined. Trace metal and organic contaminants are known to persist on glassware and effect electrochemical measurements on low surface area electrodes.³⁷ A rapid (~ 2 h) cleaning procedure in KOH and citric acid was compared to a more time-consuming (~ 32 h) and rigorous procedure in concentrated H_2SO_4 . CO_2RR CV experiments showed a 17% increase of the maximum FE_{CO} when using glassware cleaned in H_2SO_4 (74% at -0.58 V vs RHE; Fig. S23, SI) vs citric acid (57% at -0.88 V vs RHE; Fig. S22, SI). However, gradual deactivation of the RRDE was observed in both cases.

To quantify and compare the deactivation rates of FE_{CO} and j_{CO} in systems of different purity, CA RRDE measurements were performed from $E_{\text{disk}} = -0.4$ to -1.0 V vs RHE in 100 mV increments (section S16, SI). Deactivation rates at each disk potential were calculated by the linear slope between the FE_{CO} or j_{CO} 30 s and 5 min of the CA measurement (section S16, SI), and the results are shown in Fig. 8. Increasing the NaHCO_3 reagent purity from 99.7% to 99.999% noticeably reduces the deactivation rate of FE_{CO} by ca. 30%–40% (Fig. 8a). Changing the glassware cleaning method from citric acid to H_2SO_4 provides only minor additional

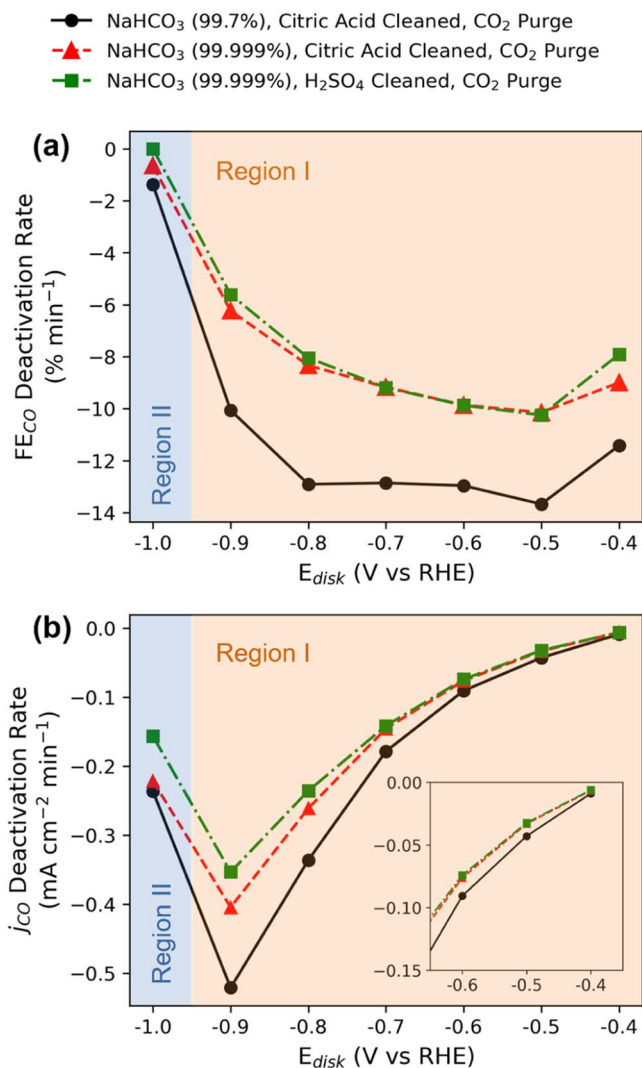


Figure 8. Deactivation rates for FE_{CO} (a) and j_{CO} (b) calculated from CA RRDE experiments on a poly-Au/Au RRDE (Figs. S33–35, SI) in electrochemical cells of differing purity. Data is an average of $n = 3$ (black circles, red triangles) or $n = 5$ (green squares) independent measurements on a freshly prepared poly-Au/Au RRDE. Regions I and II are indicated by orange and blue shading, respectively. Lines are meant to guide the eye.

suppression of the deactivation rate, indicating that reagent impurities rather than the glassware cleanliness are the predominant cause of deactivation. Even under the cleanest conditions, significant FE_{CO} deactivation rates on the order of -5% – -10% min^{-1} are still observed, so we conclude trace metal and organic contamination from the NaHCO_3 reagents and glassware are not the only sources of deactivation mechanisms present.

The FE_{CO} and j_{CO} deactivation rates were also found to depend on E_{disk} , and the trends can be separated into two potential regions, regardless of the electrolyte or glassware purity. In region I ($E_{\text{disk}} = -0.4$ to -0.9 V vs RHE), the FE_{CO} deactivation rate is fast (-5% min^{-1} or faster) and the j_{CO} deactivation rate increases with higher overpotentials. The partial current density data for region I (section S14, SI) shows that j_{CO} decreases over time while j_{H_2} increases over time, causing the high FE_{CO} deactivation rate. Conversely, region II ($E_{\text{disk}} = -0.9$ to -1 V vs RHE) shows a near-zero FE_{CO} deactivation rate and breaks the trend of increasing j_{CO} deactivation rates with increasing overpotential. The partial current density data in region II shows both j_{CO} and j_{H_2} decreasing over time with the ratio $j_{\text{CO}}:j_{\text{H}_2}$ remaining nearly constant. This comparison of regions I and II reveals that FE_{CO} and j_{CO} deactivation are both accelerated in region

I but suppressed in region II. We offer three probable explanations for this phenomenon.

First, the near-zero deactivation rates in region II may be an artifact of somewhat arbitrarily defining 30 s as one of the points used to calculate the deactivation rate. It is possible that at highly reducing overpotentials, the deactivation process is much faster and thus the electrode is mostly deactivated by 30 s. Substantially higher current flow is measured at -1 V vs RHE compared to the other potentials which would cause the electrodeposition rate of trace metals to increase. However, assessing the deactivation rate at $t < 30$ s is challenging due to non-Faradaic contributions by the formation of the electric double layer to the measured current. Thus, there is a need to model the relative contributions of double layer charging, CO₂RR, HER, and electrodeposition of contaminant metals to the overall disk current at early times of the CA experiment.

Second, the switch from region I to II may be caused by an interfacial pH effect that changes the predominant buffer reaction at the electrode interface. RRDE-based interfacial pH measurements under similar conditions (RRDE with poly-Au disk electrode, CO₂ sat. 0.1 M NaHCO₃, $\omega = 2500$ rpm), by Liu et al. found that the disk pH increases from 6.8 to 11.4 when cycling between 0 and -1.0 V vs RHE. Conversion of the predominant buffer species from CO₂/HCO₃⁻ to HCO₃⁻/CO₃²⁻ occurred at a current density of approximately -0.25 mA cm⁻² and $E_{disk} = -0.5$ V vs RHE which has also been shown to affect the predominant proton donor for HER.¹⁵ While the shift between region I and region II in this work occurs at much higher overpotentials (-1.0 V vs RHE), the FE_{CO} deactivation rate gradually decreases with increasing overpotential starting at $E_{disk} = -0.5$ V vs RHE.

Lastly, the difference between regions I and II could arise from changes to the CO oxidation reaction mechanism. Tackett et al. have shown that the ring electrode experiences the same interfacial pH shift as described previously for the disk electrode, especially at low current densities ($j_{disk} \leq 10$ mA cm⁻²).²³ The shift to more alkaline local pH with increasing CO₂RR overpotential will alter the CO oxidation mechanism from being H₂O mediated to CO₃²⁻ mediated.⁵⁷ Future work should establish the stability of COOR on the Au ring electrode in the pH range 6.8 to 11 to determine whether a shift in COOR mechanism could cause apparent FE_{CO} deactivation. Furthermore, coupling these RRDE measurements with online mass spectrometry to analyze gaseous products could deconvolute contributions of CO production at the disk from CO detection at the ring to the overall FE measurement.

Conclusions

CO₂RR selectivity measurements by RRDE are highly sensitive to electrolyte conditions making this technique appropriate for studying electrolyte effects on electrocatalytic activity and selectivity. However, this high sensitivity also requires that experimental conditions are carefully controlled to ensure reproducible results. Here we have reported the rapid and persistent deactivation of poly-Au/Au RRDEs with both CV and CA experiments. We found that both deactivation of CO production at the disk electrode and deactivation of CO detection at the ring electrode contribute to FE_{CO} deactivation. Periodic anodic cycling treatments were effective for temporarily re-activating RRDEs for selectivity measurement by stripping off trace metal poisons from the electrode surfaces. The effect of system purity was thoroughly investigated to reveal that the NaHCO₃ reagent purity was responsible for ca. 30% of the FE_{CO} deactivation. Further studies are needed to identify the additional deactivation mechanisms and devise strategies for eliminating deactivation.

These results highlight the need for standardized and cross-laboratory validation of CO₂RR selectivity measurements by RRDE. Researchers implementing this RRDE technique for CO₂RR selectivity measurements need to be cognizant of electrode deactivation

and its potential impacts on FEs and overall conclusions of their work. We suggest future RRDE CO₂RR selectivity studies include the following experimental details and analysis:

- Accompany CV measurements with CA measurements in the same potential range to detect deactivation. If deactivation is observed, determine the time scale over which deactivation occurs. Also consider the effect of FE_{CO} decrease over time on the data interpretation and any mechanistic conclusions.
- Report glassware cleaning and electrolyte purification protocols in detail.
- Clearly report procedures of any electrode reactivation processes. Compare FE_{CO} data with and without the activation procedure.
- If potential excursions are taken to the OER region, ensure in situ generated O₂ is either removed or has no effect on subsequent FE_{CO} measurements.
- Use XPS, electrochemical stripping, and/or equivalent methods to prove that electrode polishing protocols are sufficient to remove plated impurities from the electrode surface.
- At minimum, report the trace metal contaminants present in the system. Ideally, prove that purification methods are sufficient to remove contaminants.
- Examine the effects of purification methods on COOR stability at the ring electrode.

We encourage researchers to also pursue these measurements as round robin studies across multiple institutions, as has been previously conducted for poly-Pt RDE studies of the ORR.⁵⁸ Such comparisons will aid in the further development of RRDE as a robust technique for CO₂RR selectivity measurements.

Acknowledgments

This material is primarily based on work performed by the Liquid Sunlight Alliance, which is supported by the U.S. Department of Energy, Office of Science, Office of Basic Energy Sciences, Fuels from Sunlight Hub under Award DE-SC0021266. XPS measurements were performed, in part, at the Colorado Shared Instrumentation in Nanofabrication and Characterization (COSINC): the COSINC-CHR (Characterization), College of Engineering & Applied Science, University of Colorado Boulder. The authors would like to acknowledge the support of the staff (Dr Tomoko Borsa) and the facility that have made this work possible. This work was authored in part by the National Renewable Energy Laboratory, operated by Alliance for Sustainable Energy, LLC, for the U.S. Department of Energy (DOE) under Contract No. DE-AC36-08GO28308. M.K. acknowledges funding from the National Science Foundation Graduate Research Fellowship under Grant DGE2040434. R.A.W. acknowledges funding by the U.S. Department of Energy, Office of Science, Office of Workforce Development for Teachers and Scientists (WDTS) under the Science Undergraduate Laboratory Internship (SULI) program. The views expressed in the article do not necessarily represent the views of the DOE or the U.S. Government. The U.S. Government retains and the publisher, by accepting the article for publication, acknowledges that the U.S. Government retains a nonexclusive, paid-up, irrevocable, worldwide license to publish or reproduce the published form of this work, or allow others to do so, for U.S. Government purposes. We thank Dr Akansha Goyal for helpful discussions on experimental set up; Jason Zack for training in glassware cleaning and RDE/RRDE operation; and Rana Chan and Colton Paul for advice on Python code for data analysis.

ORCID

Maria Kelly  <https://orcid.org/0000-0002-7625-9655>
 Melissa E. Kreider  <https://orcid.org/0000-0003-1750-6860>
 Wilson A. Smith  <https://orcid.org/0000-0001-7757-5281>

References

- D. S. Mallapragada et al., *Joule*, **7**, 23 (2023).
- Z. J. Schiffer and K. Manthiram, *Joule*, **1**, 10 (2017).
- P. De Luna et al., *Science*, **364**, eaav3506 (2019).
- Y. Hori, *Modern Aspects of Electrochemistry*, ed. C. G. Vayenas et al. (Springer, New York, NY) 89 (2008).
- M. G. Kibria et al., *Adv. Mater.*, **31**, 1807166 (2019).
- D. Segets, C. Andronescu, and U.-P. Apfel, *Nat. Commun.*, **14**, 7950 (2023).
- N. Dutta, D. Bagchi, G. Chawla, and S. C. Peter, *ACS Energy Lett.*, **9**, 323 (2024).
- K.-H. Wu et al., *ChemElectroChem*, **7**, 4417 (2020).
- F. Zhang and A. C. Co, *J. Electrochem. Soc.*, **167**, 046517 (2020).
- A. Peroff, (2020), (<https://pineresearch.com/blog/practical-choosing-potentiostat/> accessed 2024-06-04).
- A. W. Colburn, K. J. Levey, D. O'Hare, and J. V. Macpherson, *Phys. Chem. Chem. Phys.*, **23**, 8100 (2021).
- V. Lates, A. Falch, A. Jordaan, R. Peach, and R. J. Kriek, *Electrochim. Acta*, **128**, 75 (2014).
- X. Zhu et al., *Electrochim. Acta*, **283**, 1037 (2018).
- A. Goyal, G. Marcandalli, V. A. Mints, and M. T. M. Koper, *J. Am. Chem. Soc.*, **142**, 4154 (2020).
- G. Marcandalli, A. Goyal, and M. T. M. Koper, *ACS Catal.*, **11**, 4936 (2021).
- P. Chauhan et al., *J. Phys. Chem. C*, **127**, 16453 (2023).
- A. Wadas et al., *Russ. J. Electrochem.*, **53**, 1194 (2017).
- R. E. Vos and M. T. M. Koper, *ChemElectroChem*, **9**, e202200239 (2022).
- O. van der Heijden, S. Park, R. E. Vos, J. J. J. Eggebeen, and M. T. M. Koper, *ACS Energy Lett.*, **9**, 1871 (2024).
- A. J. Bard, L. R. Faulkner, and H. S. White, *Electrochemical Methods: Fundamentals and Applications* 3rd ed. (Wiley, Hoboken, NJ) (2022).
- F. Zhang and A. C. Co, *Angew. Chem. Int. Ed.*, **59**, 1674 (2020).
- X. Liu, M. C. O. Monteiro, and M. T. M. Koper, *Phys. Chem. Chem. Phys.*, **25**, 2897 (2023).
- B. M. Tackett, D. Raciti, N. W. Brady, N. L. Ritzert, and T. P. Moffat, *J. Phys. Chem. C*, **126**, 7456 (2022).
- D. Wielend, H. Neugebauer, and N. S. Sariciftci, *Electrochem. Commun.*, **125**, 106988 (2021).
- A. Kerschbaumer et al., *Catal. Sci. Technol.*, **13**, 834 (2023).
- Z. Cui, M. A. Marx, M. N. Tegomoh, and A. C. Co, *ACS Energy Lett.*, **8**, 5201 (2023).
- A. Wuttig and Y. Surendranath, *ACS Catal.*, **5**, 4479 (2015).
- H. T. Ahangari and A. T. Marshall, *Electrocatalysis*, **11**, 25 (2020).
- G. Smith and E. J. F. Dickinson, *Nat. Commun.*, **13**, 6832 (2022).
- Y. Hori et al., *Electrochim. Acta*, **50**, 5354 (2005).
- B. Jermann and J. Augustynski, *Electrochim. Acta*, **39**, 1891 (1994).
- G. Kyriacou and A. Anagnostopoulos, *J. Electroanal. Chem.*, **322**, 233 (1992).
- K. W. Frese, *Electrochemical and Electrocatalytic Reactions of Carbon Dioxide*, ed. B. P. Sullivan (Elsevier, Amsterdam) 145 (1993), <https://sciencedirect.com/science/article/pii/B9780444883162500103>.
- D. W. DeWulf, T. Jin, and A. J. Bard, *J. Electrochem. Soc.*, **136**, 1686 (1989).
- H. Yano, F. Shirai, M. Nakayama, and K. Ogura, *J. Electroanal. Chem.*, **533**, 113 (2002).
- P. Kedzierzawski and J. Augustynski, *J. Electrochem. Soc.*, **141**, L58 (1994).
- K. Shinozaki, J. W. Zack, R. M. Richards, B. S. Pivovar, and S. S. Kocha, *J. Electrochem. Soc.*, **162**, F1144 (2015).
- Programming Manual PROFITRONIC PG 88535 Version 1.0*. Miele Professional (2011).
- K. Y. Leung and C. C. L. McCrory, *ACS Appl. Energy Mater.*, **2**, 8283 (2019).
- J. A. Z. Zeledón, A. Jackson, M. B. Stevens, G. A. Kamat, and T. F. Jaramillo, *J. Electrochem. Soc.*, **169**, 066505 (2022).
- M. C. O. Monteiro and M. T. M. Koper, *Electrochim. Acta*, **325**, 134915 (2019).
- J. G. Vos and M. T. M. Koper, *J. Electroanal. Chem.*, **850**, 113363 (2019).
- M. Łukaszewski, M. Soszko, and A. Czerwiński, *Int. J. Electrochem. Sci.*, **11**, 4442 (2016).
- M. C. O. Monteiro et al., *Nat. Catal.*, **4**, 654 (2021).
- M. Schreier, Y. Yoon, M. N. Jackson, and Y. Surendranath, *Angew. Chem. Int. Ed.*, **130**, 10378 (2018).
- H. Angerstein-Kozłowska, B. E. Conway, B. Barnett, and J. Mozota, *J. Electroanal. Chem.*, **100**, 417 (1979).
- W. Wu et al., *Adv. Mater.*, **37**, 2312894 (2024).
- C.-T. Dinh et al., *Science*, **360**, 783 (2018).
- P. Lobaccaro et al., *Phys. Chem. Chem. Phys.*, **18**, 26777 (2016).
- R. Shiratsuchi, S. Ishimaru, and G. Nogami, *Denki Kagaku*, **66**, 668 (1998).
- H. Kita, H. Nakajima, and K. Hayashi, *J. Electroanal. Chem.*, **190**, 141 (1985).
- P. Diao, J. Wang, D. Zhang, M. Xiang, and Q. Zhang, *J. Electroanal. Chem.*, **630**, 81 (2009).
- Chelex 100 and Chelex 20 Chelating Ion Exchange Resin Instruction Manual. Bio-Rad Laboratories*, <https://bio-rad.com/sites/default/files/webroot/web/pdf/lsr/literature/LIT200.pdf> (accessed 2024-06-10).
- C. L. Brosseau et al., *Nat. Rev. Methods Primers*, **3**, 1 (2023).
- H. Feng, X. Xu, Y. Du, and S. X. Dou, *Electrochem. Energ. Rev.*, **4**, 249 (2021).
- G. H. Simon, C. S. Kley, and B. R. Cuenya, *Angew. Chem. Int. Ed.*, **60**, 2561 (2021).
- G. Marcandalli, M. Villalba, and M. T. M. Koper, *Langmuir*, **37**, 5707 (2021).
- S. S. Kocha et al., *Electrocatalysis*, **8**, 366 (2017).